A Series of Lanthanide–Organic Frameworks Based on 2-Propyl-1H-imidazole-4,5-dicarboxylate and Oxalate: Syntheses, Structures, Luminescence, and Magnetic Properties

ARTICLE *in* CRYSTAL GROWTH & DESIGN · FEBRUARY 2010

Impact Factor: 4.89 · DOI: 10.1021/cg901391y

DOI: 10.1021/cg901391y

CRYSTAL GROWTH & DESIGN Article

2010, Vol. 10 1399–1408

A Series of Lanthanide−Organic Frameworks Based on 2-Propyl-1H-imidazole-4,5-dicarboxylate and Oxalate: Syntheses, Structures, Luminescence, and Magnetic Properties

Xun Feng,[†] Jianshe Zhao,*[,†] Bin Liu,[†] Liya Wang,*[,‡] Seikweng Ng,[§] Gai Zhang,[†] Jiange Wang,[‡] Xinge Shi,[‡] and Yongyong Liu[†]

[†]*Key Laboratory of Synthetic and Natural Functional Molecule Chemistry of Ministry of Education, College of Chemistry and Materials, Northwest University, Xi'an, 710069, P. R. China,* [‡]*College of Chemistry and Chemical Engineering, Luoyang Normal University, Luoyang, 471022, P. R. China, and* [§]*Department of Chemistry, University of Malaya, Kuala Lumpur, 50603, Malaysia*

Received November 5, 2009; Revised Manuscript Received January 20, 2010

ABSTRACT: A family of self-assembly lanthanide−organic coordination polymers with both rigid and flexible ligands formulated as $\{[Ln_2(Hpimda)_2(\mu_4\text{-}C_2O_4)\cdot 2H_2O]\cdot 4H_2O\}_n$ (Ln = Sm (**1**), Eu (**2**), Tb (**3**), Dy (**4**), Ho (**5**), Er (**6**), H_3pimda = 2-propyl-1H-imidazole-4,5-dicarboxylic acid) has been synthesized from the reactions of H_3pimda with trivalent lanthanide salts in the presence of oxalate as coligand. X-ray diffraction analysis reveals that these complexes are isomorphous and isostructural, and each forms a novel three-dimensional (3D) frameworks structure, in which the metalloligands' two-dimensional (2D) networks were constructed from the lanthanide ion, 2-propyl-imidazole-dicarboxylate as well as oxalate ligands, and the oxalate further acts as a pillar to link the [Ln(Pimda)(oxo)] 2D grids to generate the 3D open frameworks, leaving one-dimensional channels, which are occupied by water clusters displaying an intricate array. The luminescence emission spectra of the complexes vary depending on which lanthanide ion is present. In addition, compounds **3**, **4**, and **5** exhibited weak but significant ferromagnetic couplings within the two adjacent magnetic centers bridged through oxalato, whereas dominant antiferromagnetic interaction was observed in the erbium compound of **6**, respectively.

Introduction

Multidimensional lanthanide−organic frameworks remain a worldwide topical area of research because they have been utilized in the fabrication of materials for diode lasers and optical fibers due to their high color purity and relatively long lifetimes.[1] Other applications include biomedical assays[2] and immunoassays for early detection of cancer, besides an enormous number of new structural architectures with fascinating framework topologies,[3,4] of which multifunctional ligands containing N- and O-donors have attracted great attention because they may induce diversity in the coordination modes and interesting properties.[5] Meanwhile, crystallization of specific building blocks combined with modulated fine features has resulted in a number of new hybrid functional polymers with intriguing novel topologies,[6] among which the pillared layer architectures have been proven to be an effective and controllable route to design three-dimensional (3D) frameworks with larger channels and porous structures. However, the occurrence of pillared-layer complexes with helical character is particularly rare.[7] The discovery of non-interpenetrating molecular frames is still serendipitous since the structures are found to depend on several factors such as the nature or ratio of the ligands and the metals, the non-covalent weak interactions, and the presence of guest molecules.[8] Moreover, oxalate is most widely used in crystal engineering because it is an effective synthetic approach to new networks that may serve as "templates" for new functional materials.[9] Introducing a coligand of oxalate into the lanthanide multicarboxylate system can reduce or eliminate water molecules from the coordination sphere of the central ions, hence increasing the luminescent intensity and lifetime of the materials.[10]

By contrast with a large number of lanthanide complexes containing only rigid or flexible ligands, the rare homogeneous constructions involving both semiflexible and rigid oxalate ligands always can be obtained only from the in situ reaction, in which the multi- or dicarboxylic acid were decomposed into $C_2O_4^{2-}$,[11] and most of them are reluctant to form crystals suitable for X-ray analysis. To the best of our knowledge, systematic research on the topic based on the flexible ligand as well as rigid pillar ligands is still relatively undeveloped.[3c,9a,12] Meantime, the large orbital contributions to most of lanthanide ions and the effects of the crystal field make the explanation for the nature and magnitude of $f-f$ interactions very difficult.[13] In order to further study the coordinating behavior and role of the oxalate in the self-assembly processes, and better understand the nature of $4f-4f$ magnetic interactions as well as the luminescence in these systems, we present a new family of lanthanide-organic frameworks containing both flexible dicarboxylate and rigid dianionic ligands.

Experimental Section

Materials and Physical Measurements. All reagents used in the syntheses were of analytical grade. Elemental analyses for carbon, hydrogen, and nitrogen atoms were performed on a Vario EL III elemental analyzer. The infrared spectra (4000−600 cm^{-1}) were recorded by using a KBr pellet on an AvatarTM 360 E. S. P. IR spectrometer. The crystal determination was performed on a Bruker SMART APEX II CCD diffractometer equipped with graphite-monochromatized MoKα radiation (λ = 0.71073 Å). Thermogravimetry-differential thermal analysis was recorded using a

*To whom correspondence should be addressed. E-mail: jszhao@nwu.edu.cn (J.Z.); wlya@lynu.edu.cn (L.W.).

Published on Web 02/09/2010

Table 1. Crystal Data and Structure Refinement for Complexes 1−6[a]

compounds no.	1	2	3	4	5	6
chemical formula	$C_{18}H_{28}N_4O_{18}Sm_2$	$C_{18}H_{28}N_4O_{18}Eu_2$	$C_{18}H_{28}N_4O_{18}Tb_2$	$C_{18}H_{28}O_{18}N_4Dy_2$	$C_{18}H_{28}O_{18}N_4Ho_2$	$C_{18}H_{28}O_{18}N_4Er_2$
formula weight	889.14	894.35	904.26	913.14	918.96	922.96
temperature(K)	296(2)	296(2)	296(2)	296(1)	296(2)	296(2)
crystal system	monoclinic	monoclinic	monoclinic	monoclinic,	monoclinic	monoclinic
space group	$P2(1)/c$	$P2(1)/c$	$P2(1)/c$	$P2(1)/c$	$P2(1)/c$	$P2(1)/c$
unit cell dimensions (Å, °)	a = 8.7976(8)	a = 8.7700(11)	a = 8.7728(8)	a = 8.7723(10)	a = 8.7791(8)	a = 8.7553(11)
	b = 14.1420(13)	b = 14.0506(17)	b = 13.9842(13)	b = 13.9416(16)	b = 13.8905(13)	b = 13.8243(17)
	c = 11.9160(11)	c = 11.8427(15)	c = 11.7871(11)	c = 11.7566(14)	c = 11.7377(11))	c = 11.6778(15)
	β = 93.3290(10)	β = 93.1780(10)	β = 92.8070(10)	β = 92.7160(10)	β = 92.5680(10)	β = 92.4680(10)
V (Å^3)	1480.0(2)	1457.1(3)	1444.3(2)	1436.2(3)	1429.9(2)	1412.1(3)
Z	2	2	2	2	2	2
ρ (g cm^{-3})	1.995	2.029	2.079	2.112	2.133	2.171
F(000)	864	864	872	880	884	888
GOF	1.072	0.974	1.039	1.084	1.004	1.056
R_1, wR_2 [$I > 2\sigma(I)$]	0.0170, 0.0431	0.0295, 0.0580	0.0173,0.0417	0.0171, 0.0417	0.0134, 0.0326	0.0311, 0.0335
R_1, wR_2 (all data)	0.0188, 0.0441	0.0411, 0.0609	0.0200, 0.0431	0.0191, 0.0426	0.0143, 0.0330	0.0814, 0.0836
residuals (e Å^{-3})	0.621, −0.607	0.659, −0.814	0.680, −0.732	0.635, −0.721	0.507, −0.512	2.241, −1.487

[a] $R = \sum||F_0| - |F_c||/\sum|F_0|$, $wR = \{\sum[w(F_0^2 - F_c^2)^2]/\sum(F_0^2)^2\}^{1/2}$.

SDT 2960 simultaneous thermal analyzer (DTA Instruments, New Castle, DE) in N_2 atmosphere at a heating rate of 10 °C min^{-1} from 20 to 900 °C. Luminescence spectra of the complexes in a 1 cm quartz spectrophotometer fluorescence cell (Starna) in methanol were run on a Cary Eclipse fluorescence spectrophotometer. Variable-temperature magnetic susceptibilities were measured using a MPMS-7 SQUID magnetometer. Diamagnetic corrections were made with Pascal's constants for all constituent atoms.

Syntheses of the Complexes 1−6. {**[Sm$_2$(Hpimda)$_2$(μ_4-C$_2$O$_4$)·8H$_2$O]·2H$_2$O**}$_n$ **(1).** H_3pimda acid (0.040 g, 0.2 mmol) and ammonium oxalate (0.0152 g, 0.1 mmol) in a solution of water/alcohol (v/v = 1.5, 10 mL) of NaOH (0.004 g, 0.1 mmol) were mixed with an aqueous solution (10 mL) of $Sm(NO_3)_3 \cdot 6H_2O$ (0.078 g, 0.2 mmol). After stirring of the solution for 20 min in air, the pH value was adjusted to 6.0 with triethyleneamine, and the mixture was placed into 25 mL Teflon-lined autoclave under autogenous pressure being heated at 150 °C for 72 h. And then the autoclave was cooled over a period of 24 h at a rate 5 °C/h. After filtration, the product was washed with distilled water and then dried, and colorless crystals of **1** were obtained suitable for X-ray diffraction analysis with yield: 0.031 g (34%) based on Sm(III). Elemental analysis (%): calcd for $C_9H_{14}N_2O_9Sm$: C 24.31, H 3.17, N 6.30; found: C 24.42, H 3.25, N 6.34. IR (KBr pellet, cm^{-1}): 3481s, 3183br, 2917s, 2168s, 1619s, 1434vs, 1379vs, 1192s, 1091 m, 918s, 791s, 770 m, 662s, 607 m, 452 m.

{**[Eu$_2$(Hpimda)$_2$(μ_4-C$_2$O$_4$)]·2H$_2$O·4H$_2$O**}$_n$ **(2). 2** was synthesized by a method similar to that of **1**, except that samarium nitrate was replaced by europium nitrate accordingly, and colorless crystals of **2** were isolated. Yield: 0.034 g (38%). Elemental analysis (%): calcd for $C_9H_{14}N_2O_9Eu$: C 24.23, H 3.16, N 6.27; found: C 24.24, H 3.19, N 6.28. IR (KBr pellet, cm^{-1}): 3456vs, 3056s, 2919s, 1623s, 1445s, 1374s, 1248 m, 1087s, 929vs, 797m, 661s, 467m.

{**[Tb$_2$(Hpimda)$_2$(μ_4-C$_2$O$_4$)]·2H$_2$O·4H$_2$O**}$_n$ **(3). 3** was synthesized by a method similar to that of **1**, except that samarium nitrate was replaced by terbium nitrate accordingly. Colorless crystals of **3** were obtained. Yield: 0.033 g (36%). Elemental analysis (%): calcd for $C_9H_{14}N_2O_9Tb$: C 23.85, H 3.11, N 6.18; found: C 24.34, H 3.10, N 6.23. IR (KBr pellet, cm^{-1}): 3433vs, 3256s, 2889s, 1629s, 1537s, 1448s, 1376s, 1319m, 1128s, 784m, 663s, 590w, 527m.

{**[Dy$_2$(Hpimda)$_2$(μ_4-C$_2$O$_4$)]·2H$_2$O·4H$_2$O**}$_n$ **(4). 4** was synthesized by a method similar to that of **1**, except that samarium nitrate was replaced by dysprosium nitrate accordingly. Light-yellow crystals of **4** were obtained. Yield: 0.035 g (38%). Elemental analysis (%): calcd for $C_9H_{14}N_2O_9Dy$: C 23.94, H 3.12, N 6.20; found: C 24.04, H 3.19, N 6.16. IR (KBr pellet, cm^{-1}): 3457vs, 3082s, 2958s, 1617vs, 1476s, 1344s, 1318 m, 1278s, 1190s, 1069 m, 912s, 729s, 470 m.

{**[Ho$_2$(Hpimda)$_2$(μ_4-C$_2$O$_4$)]·2H$_2$O·4H$_2$O**}$_n$ **(5). 5** was synthesized by a method similar to that of **1**, except that samarium nitrate was replaced by holmium nitrate accordingly, and yellow crystals of **5** were obtained. Yield: 0.039 g (43%). Elemental analysis (%): calcd for $C_9H_{14}N_2O_9Ho$: C 23.54, H 3.07, N 6.10; found: C 24.01, H 3.09, N 6.15. IR (KBr pellet, cm^{-1}): 3547vs, 2952s, 1609s, 1577s, 1421s, 1380vs, 1108 m, 923s, 857s, 662m, 589s, 438 m.

{**[Er$_2$(Hpimda)$_2$(μ_4-C$_2$O$_4$)]·2H$_2$O·4H$_2$O**}$_n$ **(6). 6** was synthesized by a method similar to that of **1**, except that samarium nitrate was replaced by erbium nitrate accordingly. Pink crystals of **6** were obtained. Yield: 0.037 g (39%). Elemental analysis (%): calcd for $C_9H_{14}N_2O_9Er$: C 23.42, H 3.06, N 6.07; found: C 23.64, H 3.13, N 6.12. IR (KBr pellet, cm^{-1}): 3623vs, 3176s, 2964m, 1583vs, 15371s, 1454s, 1384m, 1253s, 1122m, 876s, 685m, 522s, 429m.

Crystallographic Data Collection and Refinement. Single-crystal diffraction data of **1−6** were collected on a Bruker SMART APEX CCD diffractometer with graphite-monochromated Mo Kα radiation (λ = 0.71073 Å) at room temperature. The structures were solved using direct methods and successive Fourier difference synthesis (SHELXS-97), and refined using the full-matrix least-squares method on F^2 with anisotropic thermal parameters for all non-hydrogen atoms (SHELXL-97). An empirical absorption correction was applied using the SADABS program. In the structures, the disordered propyl carbon atoms of the Hpimda^{2-} ligand were restrained in order to obtain reasonable thermal parameters. The hydrogen atoms of organic ligands were placed in calculated positions and refined using a riding on attached atoms with isotropic thermal parameters 1.2 times those of their carrier atoms. The water hydrogen atoms were located from difference maps and refined with isotropic thermal parameters 1.5 times those of their carrier atoms. The crystallographic data and selected bond lengths and angles for **1−6** are listed in Table 1 and Table S1, Supporting Information, respectively.

Crystallographic files in CIF format have been deposited with the Cambridge Crystallographic Data Center. Copies of this information may be obtained free of charge, by quoting the publication citation and deposition numbers CCDC: 748535 (**1**), 748536 (**2**), 748537 (**3**), 748538 (**4**), 748539 (**5**) and 749200 (**6**) from the Director, CCDC, 12 Union Road, Cambridge, CB2 1EZ, U.K. (fax +44−1223−336033; e-mail: deposit@ccdc.cam.ac.uk; http://www.ccdc.cam.ac.uk).

Results and Discussion

Hydrothermal Syntheses. Hydrothermal synthesis has been widely employed to produce new porous materials with diverse structural architectures due to the unusual condition available to minimize the problems associated with ligand solubility and enhancing the reactivity of reactants. However, there are many synthetic parameters that influence the formation of metal−organic frameworks (MOFs) during the hydrothermal synthesis, which includes the chemical structure of the ligand, the inorganic counterion, the pH values, the metal-to-ligand ratio, and the reaction medium chosen. During the experiment, our first attempts to react Sm(III) salt with Hpimda^{2-} directly by a hydrothermal process with an equal quantity of sodium hydroxide in an aqueous

Scheme 1. The Coordination Fashions of Ligands Observed in Compounds 1−6

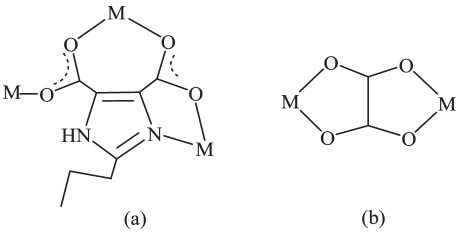

solution to deprotonate the H_3pimda gave only some precipitates or microcrystalline products that are unsuitable for single crystal X-ray diffraction analysis, which may be due to the higher pH value. Considering that the introduction of an oxalate ligand may tune the structures of the resultant metal−organic complexes, we chose ammonium oxalate as the ancillary ligand in this system, during which the pH value should not be too low in the case of the protonation of the oxalate, so the triethyleneamine was also employed instead of simply the sodium hydroxide. Fortunately, **1** was successfully isolated in its crystalline form with good yield in the appropriate condition. In order to perform a systematic investigation of the Ln(III) complexes with H_3pimda, we also changed lanthanide salts to obtain compounds **2**−**6**. Compounds **1**−**6** can be obtained between 140 and 180 °C, and once formed they are air-stable and insoluble in the common solvents.

Descriptions of the Crystal Structures of 1−6. The X-ray diffraction analyses reveal that compounds **1**−**6** are isomorphous and isostructural, and they are all three-dimensional frameworks consisting of lanthanide-organic layers pillared by oxalate ligands. Therefore, the structure of **1** was selected and described in detail to represent their frameworks. As illustrated in Figure S1 (Supporting Information), compound **1** crystallizes in the monoclinic space group $P2_1/c$, and the symmetric unit of **1** consists of two Sm(III) cations, two $Hpimda^{2-}$ dianion ligands, one oxalate ligand, and two coordinated water molecules, as well as four solvate water molecules. The coordination polyhedron around the central Sm(III) ion can be visualized as a slightly distorted dodecahedral geometry with a $Sm_1O_7N_1$ coordination mode; the two deprotonated carboxylate groups from the $Hpimda^{2-}$ ligand provide four donor oxygen atoms, the imidazolyl ring provides one nitrogen, and oxalate provides two oxygen atoms, respectively, to bond to the central ion. The remaining one site is occupied by oxygen atom of a water molecule to complete the eight-coordination configuration. Eight bonds with different lengths give rise to a distorted dodecahedral environment around the Sm(III) ion. Bond distances of Sm−O involving the central ion vary from 2.325(2) to 2.486(2) Å and the Sm−N distance is 2.602(2) Å, respectively, which are closely similar to those observed in several related species.[3c,15]

The fully deprotonated $Hpimda^{2-}$ anion acts as a pentadentate ligand in **1** and adopts a μ_3-*k*N, O: *k*O, O′: *k*O′ mode connecting three Sm(III) centers in bis-(bridging) bidentate and one monodentate modes (Scheme 1a); both carboxyl groups adopt the bis-monodentate coordination modes, and each 4-carboxylate group of $Hpimda^{2-}$ ligand links to two adjacent Sm(III) atoms to form a dimer in an anti-anti chelating mode, and the separation of Sm···Sm is 6.337 Å. The oxalate propagates these dimers into a corrugated-shape polymeric chain approximately along the crystallographic

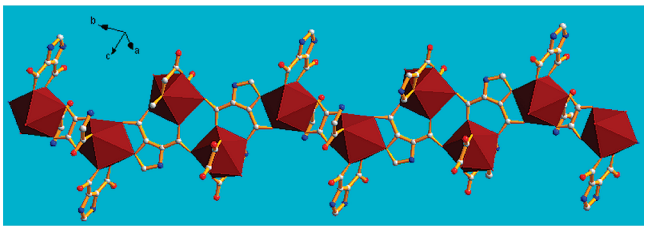

Figure 1. Polyhedral view of the Sm(III) ion and its corresponding centrosymmetric atoms alternately linked by $Hpimda^{2-}$ and oxalate ligands to lead to an infinite corrugated-shaped structure.

b axis as described in Figure 1. The oxalate ligand acts as a bidentate chelating ligand linking two metal nodes (Scheme 1b). The $Hpimda^{2-}$ ligand is three connected linking to three Sm(III) ions with a vertex symbol of (4.5.6), and the Sm(III) ion is four-connected linking to three neighboring Sm(III) by $Hpimda^{2-}$ as well as one Sm(III) via the oxobridged ligand. Then, these chains are further connected into a spectacular 2D grid by the 5-carboxylate group of the $Hpimda^{2-}$ ligand, and the 5-carboxylate group adopts a syn-anti mode to link two metal ions. The two adjacent sheets are further connected by oxalate to generate the 3D frameworks, as illustrated in Figure S2, Supporting Information. An alternate description in the cationic layer is two adjacent Sm(III) ions are first linked into a dimer through the $Hpimda^{2-}$ ligand, and the next two adjacent Sm(III) ions alternately are linked through the μ_4-oxobridged anion a little out of plane to produce a dimer, then the three adjacent dimers are arranged alternately in a Sm_6 hexagonal ring as the secondary building unit (SBU). Six Sm(III) ions are almost coplanar, and the Sm···Sm···Sm angles are within the range from 97.33(2) to 122 0.05(9)°, while the adjacent Sm(III)···Sm(III) distances vary from 6.337(2) to 6.808(5) Å. Thus, the sheets can be represented topologically by the alternating $[Ln_2(Hpimda)_2]_n$ "hexagonal circle" SBUs, and the connections between them as an order of (3, 3) net (see Figure 2). The hexagonal units propagate infinitely along the *bc* plane to generate a 2D grid, which are further assembled into the 3D non-interpenetration porous framework via oxalate and $Hpimda^{2-}$ bridged ligands acting as pillar, and the coordination fashions of the oxalate in the complex differ essentially from those of the analogous lanthanide oxalate-phosphonates in which the oxalate just acts as a linker.[10,16] As described in Figure 3, the $[C_2O_4]^{2-}$ dianion connects two neighboring Sm^{3+} using a bis-bidentate bridging mode to give rise to a zigzag chain structure along the crystallographic *b* direction.

At the same time, the lanthanide ions tethered by flexible $Hpimda^{2-}$ as well as oxalate ligands form a one-dimensional (1D) chain, and these chains display a 1D left-handed (M) helical infinite chain around the 2_1 screw axis along the *ab* plane as depicted in Figure 4a, with a pitch of 11.349 Å. The remaining coordination sites of Sm(III) within the chain were taken by oxalate anions like parallels, so the neighboring chains have to be a right-handed (P) helix for the coordination of the oxalate anion in the primal formed left-handed chain to the Sm(III) in the neighboring helix. This means the left-handed chirality (P) of the original formed chain is transferred oppositely to the adjacent right-handed chirality (M) of helix by the coordination of dicarboxylate bridges of the $Hpimda^{2-}$ ligand linked by the central lanthanide ions,[17] as displayed in Figure 4b. Because left-handed and right-handed helical chains coexist in the

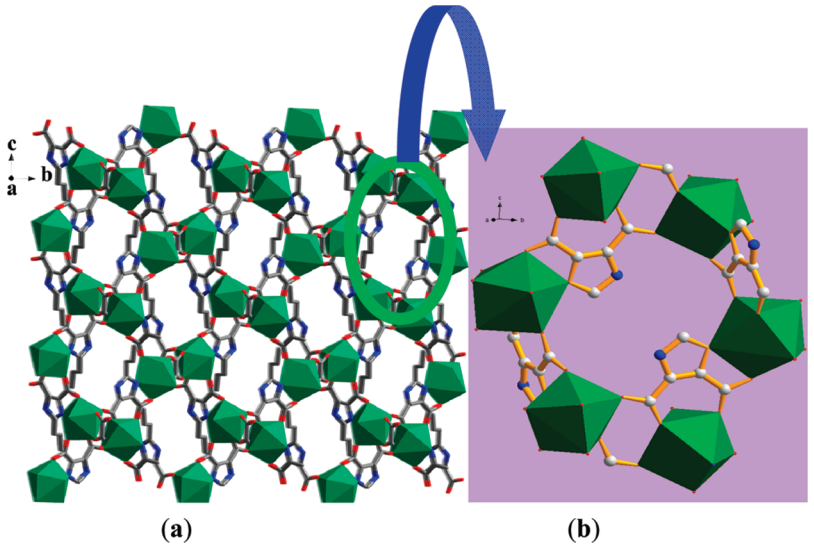

Figure 2. (a) Polyhedron view of a spectacular 2D network in **1** down the *a*-axis. (b) lllustration of an individual Sm_6 hexagonal ring viewed approximately down the *a*-axis in **1**.

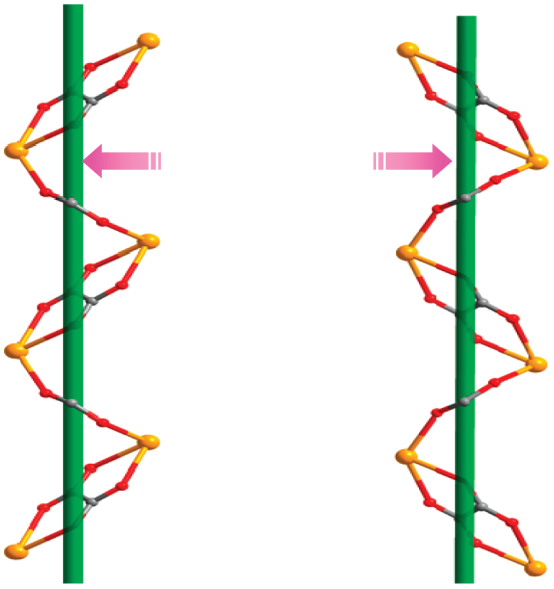

Figure 3. Ball and stick presentation of adjacent oxo-Ln-oxo zigzag chains along the *b*-axis in **1**.

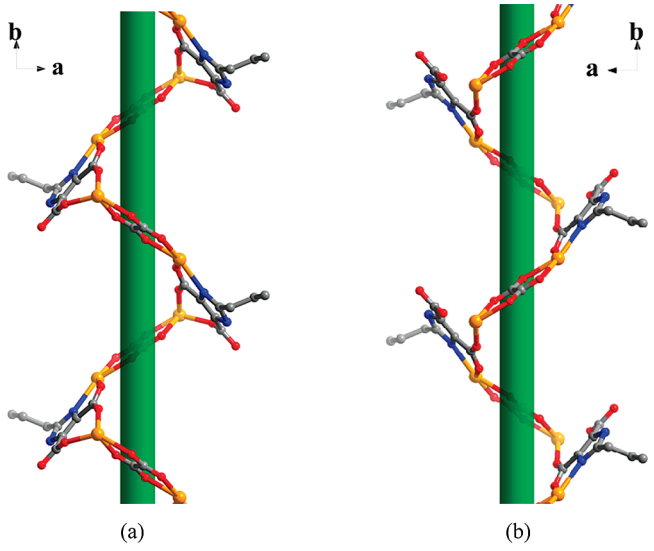

Figure 4. Ball-and-stick illustration of the left- and right-hand helical oxo-Ln-Hpimda chains viewed along the *c* axis in **1**.

crystal structure, the whole crystal is racemic and does not exhibit chirality.[18] On the basis of the discussion above, the occurrence of the helical structure may be attributable to the flexibility of the $Hpimda^{2-}$ ligand.

As mentioned above, each $Hpimda^{2-}$ ligand in **1** acts a three-connected node linking to three Sm(III) ions with a vertex symbol of (4.5.6), the oxalate ligands simply acting as a linker between two metal nodes, so the $Hpimda^{2-}$ ligand is three connected and Sm(III) ion is four-connected node. From the viewpoint of topology, the structure is a binodal (three, four) connected net, with the vertex symbol of $(4.5^2.6.7^2)(4^2.5^3.6^3.7.9)(4^2.5^3.7)(4^3.5.6^2.7.8^2.9)(5^2.6^2.9^2)(5)$, which represents a new network topology.[19] To further reduce this 3D structure, the familiar dimeric Sm(III) units can be considered as one node, and the oxobridged ligand was treated as a linker. In this condition, the robust network with a Schläfli symbol of $(4.8^2)(4.6^5)$ is generated, as shown in Figure 5a.

In the 3D frameworks structure, the oxalate further acts as pillar to link the $[Ln(Hpimda^{2-})(oxo)]$ 2D networks to form 3D open frameworks, leaving a 1D cationic channel present along the *b* axis (dimensions 11.141 × 11.943 $Å^2$) in the frameworks; the Sm(III) ions, alternately connected by oxalate anions and $Hpimda^{2-}$ ligands, act as walls of the channels, and the channels are filled by the coordinated water as well as lattice water molecules as illustrated in Figure 5b, which are stabilized by hydrogen bonds interactions. The total potential solvent volume is 273.2 $Å^3$, accounting for ca. 17.1% of per cell volume of 1480.0 $Å^3$ calculated by the Platon programs.[20] Careful inspection of the 1D channel suggests the atom Ow8 is hydrogen bonded to carboxylate O1 atom of other chains, O(8w)−H(3w8)···O(1), [O−O = 2.747(3) Å, O−H···O = 173.6°], while the O(9w) is hydrogen-bonded to two more water molecules (O(7w), O(8w)) forming a hexameric water cluster with three other water molecules related by a center of symmetry and belonging to the different polymeric chains, among which the two adjacent included waters form the

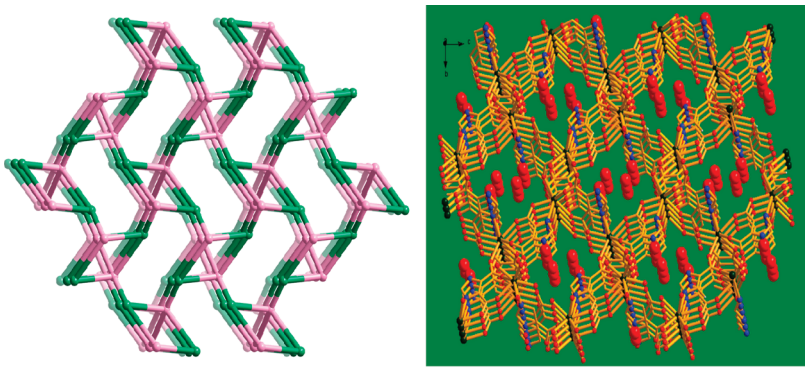

(a) (b)

Figure 5. (a) Schematic illustration of the topological crystalline framework of **1** with (3,4)-connected type. Color codes: green balls represent three-connected $Hpimda^{2-}$ ligands; pink balls represent four connected Sm(III) ions. (b) Perspective view of the three-dimensional framework of complex **1** with the elliptical one-dimensional tunnels encapsulating water molecules represented by red spheres along the *100* direction. (The reader is referred to the web version of this article.)

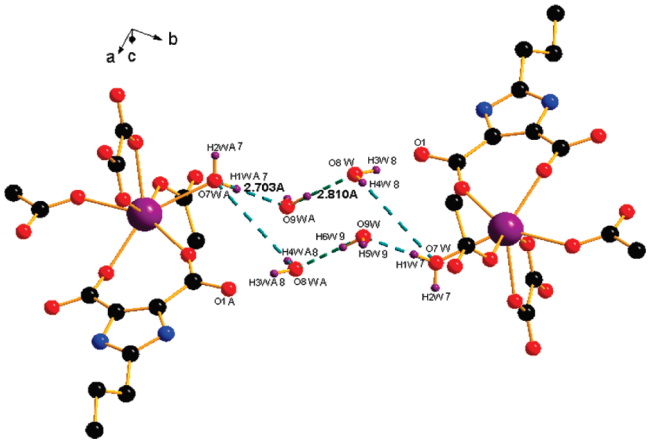

Figure 6. A perspective view of the hexameric water cluster connecting two Sm(III) ions in **1** approximately along the *ab* plane.

dimer units through the hydrogen-bonding showing the O(w7)···O(w9) distance of 2.703 Å, and the hexameric clusters form an ice-like chair conformation connecting two Sm(III) ions in the 1,4-position as depicted in Figure 6. In the chair-shape conformations, the O···O distances are 2.703 and 2.810 Å, respectively. The value observed here is much less than the standard value of 2.85 Å in regular ice,[21] and these water clusters are stabilized in the apertures of this 3D construction by the hydrogen bonds, which involves the oxygen atom from water molecules, oxalate anions, and the carboxylate oxygen atoms from the $Hpimda^{2-}$ ligands, where the O(9w)−H(6w)···O(8w) angle was nearly linear (177.83°). The bond angles in the hexamer cluster O(9wA)−O(8w)−O(7w) and O(8wA)−O(9w)−O(7w) are found to be 109.267° and 106.875°, respectively, in **1**, which deviates little from the corresponding value of 109.28° in the hexagonal ice. This hexameric clusters array can also observed in the analogous lanthanide complex, and the possible effect of the presence of water dimers on the conformation of the hexamer cluster would be minimum in the present structures.[22] These water clusters can be regarded as the simplest supramolecular analogue of cyclohexane, and it can help us to understand how the bulk water plays an important role to stabilize the native conformation of the biomolecules in the self-assembly process depending on many noncovalent interactions. In **1**, the water molecule O(w8) behaves as H donors, O(w9) as H acceptors, while O(w7) behaves as an acceptor as well as a donor in the hydrogen bonding scheme. The water molecules of the dimeric and hexameric clusters are hydrogen bonded to carboxylate O atoms of different polymeric chains resulting in an overall 3D network structure, and the water clusters occupy the 3D channels. Element analyses and thermogravimetric analyses have been used to confirm the presence of water cluster in these compounds.

Table 2. Comparison of the Ln···Ln Metal Distances for the Series of Compounds

complexes	separation of Ln···Ln bridged via oxalate (Å)	separation of Ln···Ln bridged via $Hpimda^{2-}$ (Å)
1 (Sm)	6.337	6.808
ref **24** (Gd)	6.299	6.774
2 (Eu)	6.296	6.767
3 (Tb)	6.266	6.737
4 (Dy)	6.242	6.721
5 (Ho)	6.227	6.707
6 (Er)	6.194	6.675

It should be pointed out that in the present work from the light rare earth samarium complex of **1** to the heavy rare earth erbium complex of **6**, they all exhibit the same 3D porous structure, which is different from the other reported lanthanide coordination polymers with diversity structure based on the multi N,O-donor ligand.[16a,23] However, similarities in bonding motifs for the series of lanthanide complexes and the recently studied gadolinium(III) complex[24] allow us to compare the metal−ligand distances in the same array. Table S1, Supporting Information, compares the average bond distances for the Ln−O and Ln−N bond, and metal−metal distances could only be compared for the complexes that formed in same arrays. As the ionic radius of the metal becomes smaller in the order Sm(III) > Eu(III) > Gd(III) > Tb(III) > Dy(III) > Ho(III) > Er(III), their corresponding bond lengths decrease, consistent with the lanthanide contraction except the complex of gadolinium, which may be due to the Gd-off effect. In addition, comparative investigation on the isostructural complexes **1**−**6** has found that in the same 1D array, the Ln···Ln separation bridged by oxalate and Ln···Ln separation bridged by $Hpimda^{2-}$ also display decrease trends with increasing of elements order, which are also consistent with the lanthanide contraction,[25] as listed in Table 2.

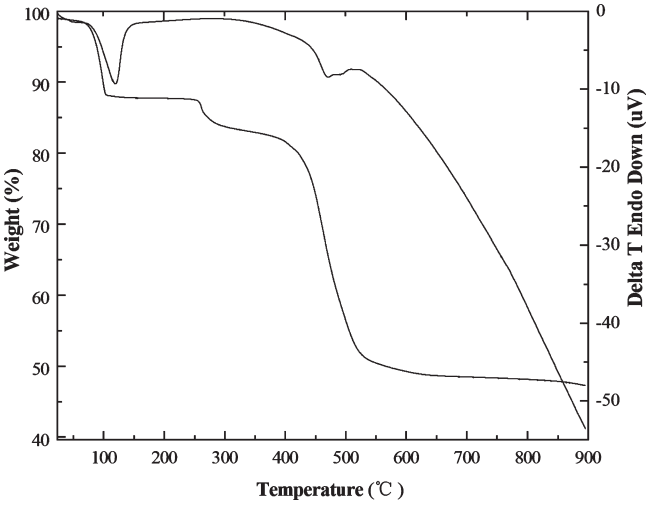

Figure 7. TG−DTA curves for complex **6**.

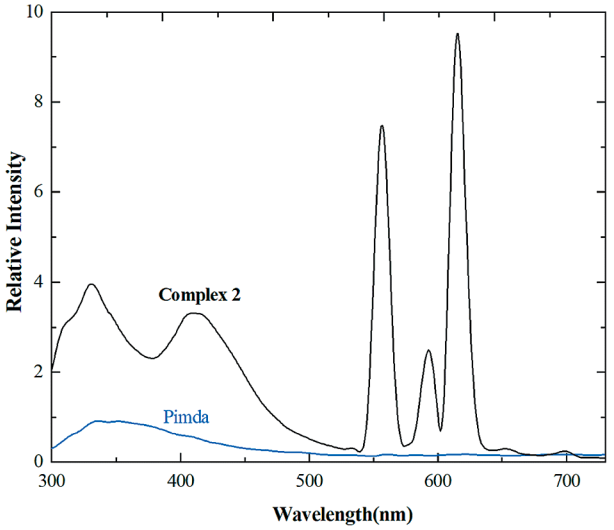

Figure 8. The photoemission spectra of the complex **2** and H_3pimda^{2-} ligand in methanol.

Thermal Properties. Thermogravimetric analysis (TGA)−differental thermogravimetric analysis (DTA) studies were performed in a N_2 atmosphere at a heating rate of 10 °C·min^{-1} for complexes **1**−**6**; they showed the almost similar TG curves, and here complex **6** was used to as a representative. As displayed in Figure 7, the TGA diagram of **6** exhibits an initial mass loss of 11.7% between 30 and 108 °C corresponding to the start with the departure of the lattice water molecules and two coordinated water molecules (calcd 11.8%), and the decomposition of **6** begins above 258 °C, from 300 to 418 °C with a weight loss of 8.74%, which is attributed to the release of the oxalate group (calcd. 9.42%). An advanced degradation process takes place after 250 °C. For **6**, the compound began to decompose upon further heating and underwent a rapid and significant weight loss of 32.4% covering the temperature from 425 to 535 °C, which corresponds to the destruction of the $Hpimda^{2-}$ organic ligands (calcd. 33.5%), consistent with the crystal structure analysis. The residue accounts for 46.05%, which is nearly in agreement with the calculated value of 45.42%, by assuming the final product is Er_2O_3. The DTA curve exhibits two strong endothermic peaks at approximately 119 and 472 °C, corresponding to the release of water molecules and decomposition of the organic fraction, respectively. Thermogravimetric analysis of compounds **1**−**5** reveals similar DT−TGA curves, which indicate three main steps of weight losses, as reported in Figure S3, Supporting Information.

Photoluminescent Properties. Taking into accounting the excellent luminescent properties of lanthanide complexes, the photoluminescence properties of the methanol suspension samples (ca. 0.01 mol/L) of **1**−**6** as well as the H_3pimda ligand were investigated at room temperature upon photoexcitation at 261, 281, 276, 284, 277, 279, and 256 nm, respectively, as reported in Figures 8 and S4, Supporting Information, respectively. Figure S4a illuminated that in the region from 320 to 450 nm (blue region), the samarium of complex **1** exhibits not only a narrow emission band with a maximum wavelength of 327 nm but also several sharp line spectra with a maximum wavelength of λ_{max} = 418 nm. The blue fluorescent emission band at λ_{max} = 418 nm corresponds to the $^2P_{5/2} \rightarrow {}^8S_0$ transition for the Sm(III) ion.[26] By comparison of the other samarium-based polymers, the emission with λ_{max} = 327 nm is assigned to a ligand-centered (LC) fluorescence, based on the emission spectrum of the free ligand.[27] The emission spectrum with a maximum wavelength of 547 nm is attributed to the characteristic emission of $^4G_{5/2} \rightarrow {}^6H_{5/2}$.[28] The europium complex of **2** showed (see Figure 8) intense luminescence with emission not only in the UV (near UV) region with two broad bands with the maximum wavelength of 329 and 423 nm; also several sharp line spectra in the red region with a maximum wavelength of λ_{max} = 556, 593, 617 nm are observed, as well as two weak peaks at 651, 702 nm, respectively. Complex **2** displays intensity red luminescence and the characteristic *f*−*f* transition of a Eu(III) ion; the strong intensities of emission at 593 and 617 nm are attributed to $^5D_0 \rightarrow {}^7F_1$ and $^5D_0 \rightarrow {}^7F_2$ transition, respectively.[29] The medium strong intense emission at 556 nm is attributed to the $^5D_0 \rightarrow {}^7F_0$ transition. The spectra is dominated by the intensity of the $^5D_0 \rightarrow {}^7F_2$ electron dipole transition; the intensity ratio of $^5D_0 \rightarrow {}^7F_2/{}^5D_0 \rightarrow {}^7F_1$ is 3.81, much higher than 0.67, a typical value for a centrosymmetric Eu(III) center. This high ratio therefore signifies that the Eu(III) ion adopts a noncentrosymmetric coordination environment without an inversion center,[30] as observed in the single crystal structure. This is also supported by the fact of the appearance of a $^5D_0 \rightarrow {}^7F_0$ transition which is forbidden in a symmetry field. The emission peaks of 629 and 702 nm correspond to the magnetic dipole transitions, both with weak intensities.[31] As depicted in Figure 8, the H_3pimda ligand displays an emission at λ_{max} = 334 nm, which is overlapped by the first emission peak of **2** in UV region, and indicates that it would be attributed to the formation of ligand-to metal charge transfer (LMCT) transition.[32] It is noteworthy that the Eu(III) complex shows a higher intense fluorescence emission than that of the free heterocyclic dicarboxylic acid ligands.[33]

Terbium complex of **3** is impressive in Figure S4b (Supporting Information), as all the transitions to the ground-state manifold from the emitting $^5D_4$ level are observed when excited at 281 nm. It emits green light and exhibits the characteristic transition of $^5D_4 \rightarrow {}^7F_J$ (J = 4−6) of the Tb(III) ion. Two intense emission bands at 493 and a sharp line emission at 549 nm correspond to $^5D_4 \rightarrow {}^7F_6$ and $^5D_4 \rightarrow {}^7F_5$ transition manifold of Tb(III) are observed, which gives an intense green luminescence, while the weaker emission bands at 585 nm originate from the $^5D_4 \rightarrow {}^7F_4$ transition.

The typical emission band at 555 nm corresponding to $^5D_4 \rightarrow {}^7F_3$ disappears due to a double-frequency effect;[34] in addition, the emission wavelength of ca. 560 nm is the most intense transition, which is also comparable with those observed in various Tb(III) contained compounds.[4d,9a,15a,35] The emission spectra of dysprosium complex **4** are displayed in Figure S4c (Supporting Information); it exhibits an intense band at 329 and 357 nm in the UV region. The emission peak is located at 329 nm, which means a blue shift of ca. 10 nm relative to that of the free H_3pimda ligand. It is tentatively assigned to the formation of LMCT transition, and the emission at 567 nm is indicative of the larger probability for the $^4F_{9/2} \rightarrow {}^6H_{13/2}$ transition of Dy(III) ion.[36] As shown in Figure S4d (Supporting Information), the holmium complex of **5** shows an emission spectra at the maximum wavelength of 328 nm and a shoulder at the 412 nm, assigned to the characteristic emission of the $^5I_8 \rightarrow {}^5G^4 + {}^3F_7$ transition of the Ho(III) ion, and a weak band emission spectrum also can be observed in the range of 550−580 nm (in the yellow region) with a maximum wavelength of 570 nm, corresponding to the characteristic emission of $^5I_5 \rightarrow {}^5I_8$ transition of Ho(III) ion.[37] As reported in Figure S4e (Supporting Information), the erbium complex of **6** showed three main emission bands in UV and green regions with the maximum wavelengths of 330, 419, and 544 nm, the first emission band is in the UV−vis region around 330 nm, since a weak similar emission with a maximum wavelength at 333 nm is also observed for the free H_3pimda ligand; according to that found in **2** and **3**, the emission band at 330 nm would be attributed to the formation of LMCT.[38] The latter corresponds to characteristic emission of $^4H_{15/2} \rightarrow {}^4I_{7/2}$ and $^4I_{15/2} \rightarrow {}^2H_{11/2}$ transitions of Er(III) ion, respectively.[39] This indicates that effective energy transfer takes place between the ligands and the lanthanide ions in **6**.

It is interesting that the complexes cannot be dissolved in common solvents (methanol included), but the lanthanide compounds in methanol solution emits bright fluorescence, which is attributed to the presence of molecular metalligand species, and both imidazole-dicarboxylate and oxalate function as activators and substantially enhance the lanthanide luminescence intensity from *f*−*f* emission.[1d,2d,3d] From the emission spectra mentioned above, it can be found that the energy transfers from the organic ligands to Tb^{3+} and Eu^{3+} ions are more effective than those to Dy^{3+}, Sm^{3+}, Er^{3+}, and Ho^{3+} ions, and the absence of the ligand-based emission in the fluorescence spectra of **1**, **2**, **5**, and **6** suggests that the energy transfer from the ligand to the lanthanide center is effective.

Magnetic Properties. The variable-temperature susceptibility measurements of complexes **3**, **4**, **5**, and **6** have been performed in the range 2−300 K at a magnetic field of 10000 G. The temperature dependencies of the magnetic susceptibilities in the form of $\chi_M T$ and χ_M vs T for complexes are given in Figures 9, S5, S6, and 10. As shown in Figure 10, at 300 K, $\chi_M T$ is equal to 22.105 cm^3 K mol^{-1}, as expected for two isolated Tb(III) ions (23.22 cm^3 K mol^{-1}, $g = 3/2$).[40] When the temperature is lowered, $\chi_M T$ increases continuously and reaches a maximum of 25.08 cm^3 K mol^{-1} at 55 K, and χ_MT, then decreases dramatically as the temperature is further lowered to 22.17 cm^3 K mol^{-1} at 2 K. Such behavior can referred to the presence of a weak ferromagnetic interaction between the Tb(III) ions in **3** beyond the temperature of 55 K. The observed decrease of $\chi_M T$ at low temperature may be due to the large anisotropy effects observed for these

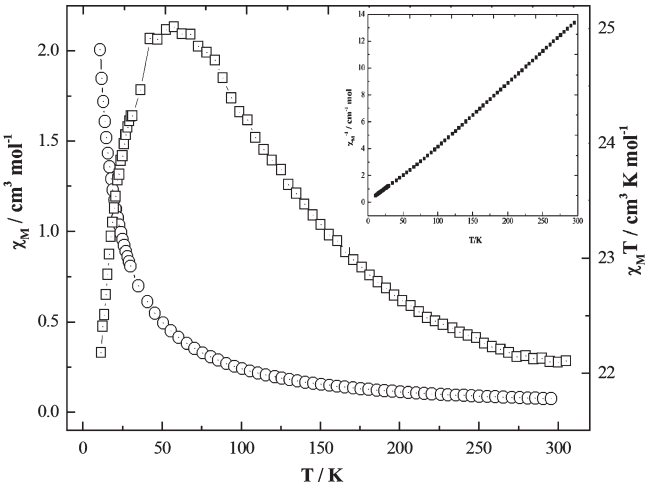

Figure 9. Plots of $\chi_M T$ (□) and χ_M (O) against temperature T for complex **3** and reciprocal molar magnetic susceptibilities χ_M^{-1} of **3** as the function of temperature (inset).

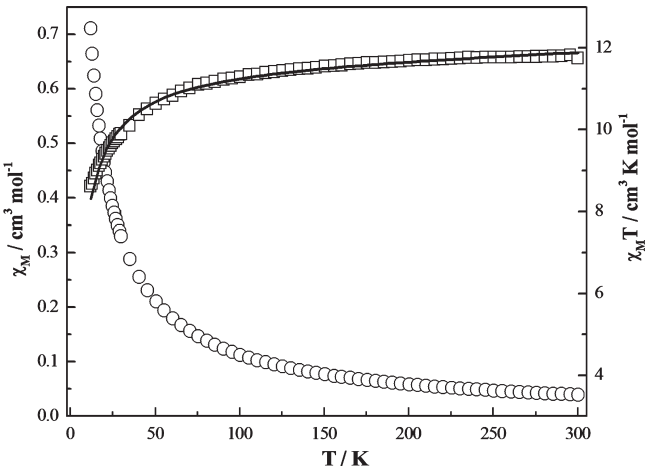

Figure 10. Temperature dependence of $\chi_M T$ (□) and χ_M (O) for complex **6**. The solid line represents the theoretical values based on equations described in the text.

lanthanides. The thermal evolution of χ_M^{-1} obeys Curie−Weiss law, $\chi_M^{-1} = C/(T - \theta)$ over the whole temperature range with Weiss constant $\theta = 4.382$ K. The Curie constant, C of 22.06 cm^3 K mol^{-1} is consistent with the theoretical value for a binuclear complex of Tb(III).[40] A similar evolution is observed in the case of **4**. As illustrated in Figure S5 (Supporting Information), $\chi_M T$ is equal to 29.56 cm^3 K mol^{-1} at 300 K, which is nearly consistent with the value expected for two isolated Dy(III) ions (28.34 cm^3 K mol^{-1}, with $g = 4/3$).[41] When the temperature is lowered, $\chi_M T$ increases slowly to 29.30 cm^3 K mol^{-1} at ca. 45 K, then rapidly decreases down to 2 K, and at this temperature, it reaches a minimum of 14.17 cm^3 K mol^{-1}, which indicates that there is a ferromagnetic coupling between the adjacent Dy(III) ions at higher temperature. The whole profile of the $\chi_M T$ vs T curve is indicative of the occurrence of an inflection effect. On one hand, the decreases in $\chi_M T$ unambiguously originate in the thermal depopulation of the highest Stark levels resulting from the splitting of the free-ion ground state $^6H_{15/2}$ by the crystal field, and on the other hand, the antagonist process must be the ferromagnetic interaction between the Dy(III) ions. Interestingly, the ferromagnetic interaction in **4** is obviously different from the situation in

the reported homodinuclear Dy(III) complex PcDyPcDyPc* (Pc = dianion of phthalocyanine, Pc* = dianion of 2, 3, 9, 10, 16, 17, 23, 24-octabutoxyphthalocyanine).[42] As for the holmium complex of **5**, $\chi_M T$ is equal to 10.71 cm^3 K mol^{-1} at 300 K, which is somewhat less than the expected spin-only value for independent spins $S = 2$ (10.61 B.M., $g = 5/4$).[41] When the temperature is lowered, $\chi_M T$ increases very slowly to 50 K ($\chi_M T$ = 11.42 cm^3 K mol^{-1}) and then decreases dramatically down to 2 K; it exhibits weak but significant ferromagnetic couplings between the adjacent Ho(III) ions bridged through carboxylato, as shown in Figure S6 (Supporting Information).

The plots of $\chi_M T$ and χ_M versus T for **6** are illustrated in Figure 10. It is worth noting that the situation of **6** is very different from the above complexes. For the former complexes, the usual decrease in the value of $\chi_M T$ is observed upon lowering the temperature, while it did not display a minimum. The $\chi_M T$ value of complex **6** at 300 K is 11.97 cm^3 mol^{-1} K, which is slightly larger than the expected spin-only value for one independent spin $S = 15/2$ (11.48 cm^3 mol^{-1} K, $g = 6/5$).[29] This can probably be ascribed to crystal-field splitting of the ground state of the Er^{3+} ion ($^4I_{15/2}$). Upon cooling the $\chi_M T$ value decreases gradually continuously to a value of 0.18 cm^3 mol^{-1} K at 2 K, and a similar phenomenon was found in the series of other lanthanide-organic frameworks with an imidazole-containing flexible ligand.[43] This feature is possibly the result of intramolecular antiferromagnetic interactions dominating the magnetic properties in the complex **6**, and/or more likely the thermal depopulation of the erbium(III) excited states (Stark sublevels of the $^2H_{11/2}$, $^4I_{13/2}$, and $^4S_{3/2}$ states).[44]

To get new insights on the magnetic properties of rare-earth mononuclear species, we investigated the temperature dependence of the magnetic susceptibility of erbium compound **6** in detail. There are two pathways of magnetic interaction in the present system, namely, (i) the adjacent two Er(III) ions bridged by the μ_4-oxobridged ions with the Er···Er separation of 6.33 Å. (ii) two Er(III) ions of adjacent chains further bridged via the $Hpimda^{2-}$ ligands with the separation of 6.81 Å. According to the crystal structure of **6** described above, the large Er···Er separation 6.33 and 6.81 Å allows us to consider that the system is treated with the mononuclear species from the magnetic point of view. As far as the existence of a strong spin−orbit coupling for Ln atoms is concerned, the magnetic data were analyzed by the free-ion approximation.

The approximate treatment equation previously derived by Andruh, and Ishikawa et al.[42,45] was applied to estimate these magnetic interactions. The second term in the right-hand side

$$\chi(J) = \frac{Ng_J^2\beta^2 J(J+1)}{3kT} + \frac{2N\beta^2(g_J-1)(g_J-2)}{3\lambda} \quad (1)$$

$$\chi = |J|/KT \quad (2)$$

of eq 1 is a temperature-independent contribution arising from the coupling between ground and excited states through the Zeeman perturbation; λ is the spin−orbit coupling parameter. In this expression, g is the Zeeman factor, N, β, k, and g have their usual meanings and J is the exchange

$$g_J = \frac{3}{2} + [S(S+1) - L(L+1)]/2J(J+1) \quad (3)$$

coupling parameter between the adjacent spins. An additional coupling parameter zJ' was added in eq 2 to take into account the magnetic behavior between the adjacent alternate chains as a molecular field approximation.[46]

$$\chi = \frac{\chi_M}{1 - \frac{2zJ'}{N\beta^2 g^2}\chi_M} \quad (4)$$

The least-squares analysis of magnetic susceptibilities data led to $J = -20.14$ cm^{-1}, $g = 0.79$, $zJ' = -0.1085$ cm^{-1}, the agreement factor $R = 1.13 \times 10^{-5}$, (R is the agreement factor defined as $R = \sum[(\chi_M T)_{obs} - (\chi_M T)_{calc}]^2/\sum[(\chi_M T)_{obs}]^2$), and the temperature dependence of the reciprocal susceptibilities ($1/\chi_M$) plot for **6** see Figure S7, Supporting Information, obeys the Curie−Weiss law [$\chi_M = C/(T - \theta)$] above 30 K with C = 21.28 cm^3 K cm^{-1}, $\theta = -7.19$ K, and $R = 1.33 \times 10^{-5}$. The Curie constant C is somewhat larger than the theoretic value of 9.8 μ_B, and the important deviation of the magnetic susceptibility with respect to the Curie law is due to the crystal field which splits the $^4I_{15/2}$ free ion ground state into eight Kramers doublets.[47] The negative θ value further supports the presence of overall weak antiferromagnetic interactions between adjacent Er^{3+} ions. The reason for the mediate J value results from the large Er(III)···Er(III) separation as well as the result of the 4f orbitals being very efficiently shielded by the fully occupied 5s and 5p orbitals and thus almost uninvolved in bonds between the neighboring lanthanide(III) ions.[48]

Conclusions

Six new lanthanide−organic frameworks based on both rigid and semiflexible ligands have been successfully isolated using the H_3impda ligand as spacer, and the oxalate as the second metal linker. In the series of MOFs metalloligands, 2D networks were constructed from the lanthanide ion, imidazole dicarboxylate as well as oxalate ligands, amongst which the oxalate further links $[Ln(pimda)(oxo)]_2$ layers to form the 3D open frameworks, leaving 1D channels filled up by guest water molecules. Informative susceptibility measurements indicate that their magnetic properties are very different, though they have the same structures. In addition, the average Ln−N and the Ln−O bond lengths decrease from **1** (samarium) to **6** (erbium) complex, as well as the Ln···Ln separation divisions, which are due to the discrepancy of lanthanide ions rather than the different orientations of dicarboxylate ligands, which are consistent with the radius decreasing with the increasing atomic number of the lanthanides. To the best of our knowledge, compounds **1**−**6** represent the first examples of a 3D lanthanide hybrid with (3,4)-connected frameworks, containing both heterocyclic dicarboxylate and oxalate ligands systematically structurally characterized. This work not only provides novel examples of 3D lanthanide hybrids but also may open up possibilities for the design of new functional materials with luminescent and magnetic properties.

Acknowledgment. We gratefully acknowledge financial support of this work by the National Natural Science Foundation of China (Nos. 20771054 and 20971104), the Ph.D. Programs Foundation of Ministry of Education of China (No. 200806970008), and Foundation of National Science and Technology Pillar Program of China (No. 2007BAB17B02).

Supporting Information Available: Coordination environment of the Sm(III) ions in complex **1**, perspective view of the 3D framework of **1**. The TGA traces for complexes **1**−**5**. The emission spectra of the complexes **1** and **3**−**6**. Plots of the temperature dependences of $\chi_M T$ and χ_M for complexes **4** and **5**, etc. This information is available free of charge via the Internet at http://pubs.acs.org.

References

(1) (a) Bunzli, J. C. G.; Piguet, C. *Chem. Soc. Rev.* **2005**, *34*, 1048. (b) Kuriki, K.; Koike, Y.; Okamoto, Y. *Chem. Rev.* **2002**, *102*, 2347. (c) Hou, H. W.; Li, G.; Li, L. K.; Zhu, Y.; Meng, X. R.; Fan, Y. T. *Inorg. Chem.* **2003**, *42*, 428. (d) Martínez-Máñez, R.; Sancenón, F. *Chem. Rev.* **2003**, *103*, 4419.

(2) (a) Aime, S.; Crich, S.; Gianolio, E.; Giovenzana, G. B.; Tei, L.; Terreno, E. *Coord. Chem. Rev.* **2006**, *250*, 1562. (b) Zhang, J. P.; Chen, X. M. *J. Am. Chem. Soc.* **2008**, *130*, 6010. (c) De Sa, G. F.; Malta, O. L.; De Mello Donega, C.; Simas, A. M. *Coord. Chem. Rev.* **2000**, *196*, 165. (d) Seward, C.; Hu, N.-X.; Wang, S. *J. Chem. Soc., Dalton Trans.* **2001**, 134.

(3) (a) Senegas, J.-M.; Bernardinelli, G.; Imbert, D.; Bünzli, J.-C. G.; Morgantini, P.-Y.; Weber, J.; Piguet, C. *Inorg. Chem.* **2003**, *42*, 4680. (b) Shi, F.-N.; Silva, L. C.; Trindade, T.; Almeida. Paz, F. A. A.; Rocha, J. *Cryst. Growth Des.* **2009**, *9*, 2098. (c) Zhang, X.-J.; Xing, Y.-H.; Han, J.; Zeng, X.-Q.; Ge, M.-F.; Niu, S.-Y. *Cryst. Growth Des.* **2008**, *8*, 3680. (d) Janiak, C. *Dalton Trans.* **2003**, 2781.

(4) (a) Reger, D. L.; Wright, T. D.; Semeniuc, R. F.; Grattan, T. C.; Smith, M. D. *Inorg. Chem.* **2001**, *40*, 6212. (b) Zaman, M. B.; Smith, M. D.; Zur Loye, H. C. *Chem. Commun.* **2001**, 2256. (c) Kitaura, R.; Seki, K.; Akiyama, G.; Kitagawa, S. *Angew. Chem., Int. Ed.* **2003**, *42*, 428. (d) Huang, Y. G.; Wu, B. L.; Yuan, D. Q.; Xu, Y. Q.; Jiang, F. L.; Hong, M .C. *Inorg. Chem.* **2007**, *46*, 1171.

(5) (a) Tao, J.; Tong, M.-L.; Shi, J. X.; Chen, X. M.; Ng, S. W. *Chem. Commun.* **2000**, 2043. (b) Li, X.; Cao, R.; Sun, Y. -Q.; Shi, Q.; Yuan, D. Q.; Sun, D.-F.; Bi, W. H.; Hong, M.-C. *Cryst. Growth Des.* **2004**, *4*, 255. (c) Wang, Z.-W.; Ji, C.-C.; Li, J.; Guo, Z.-J.; Li, Y.-Z.; Zheng, H.-G. *Cryst. Growth Des.* **2009**, *9*, 475. (d) Li, X.; Wu, B. L.; Niu, C.-Y.; Niu, Y. Y.; Zhang, H. Y. *Cryst. Growth Des.* **2009**, *9*, 3423.

(6) (a) Yaghi, O. M; Li, G. M; Li, H. L. *Nature* **1995**, *378*, 703. (b) Decurtins, S.; Schmalle, H. W.; Schneuwly, P.; Zheng, L. M.; Ensling, J.; Hauser, A. *Inorg. Chem.* **1995**, *34*, 5501. (c) Waldmann, O.; Hassmann, J.; Müller, P.; Hanan, G. S.; Volkmer, D.; Schubert, U. S. *Phys. Rev. Lett.* **1997**, *78*, 3390.

(7) (a) Kondo, M.; Miyazawa, M.; Irie, Y.; Shinagawa, R.; Horiba, T.; Nakamura, A.; Naito, T.; Maeda, K.; Utsuno, S.; Uchida, F. *Chem. Commun.* **2002**, 2156. (b) Wang, X. L.; Qin, C.; Wang, E. B.; Xu, L.; Su, Z. M.; Hu, C. W. *Angew. Chem., Int. Ed.* **2004**, *43*, 5036.

(8) (a) Zhao, B.; Yi, L.; Dai, Y.; Chen, X. Y.; Cheng, P.; Liao, D. Z.; Yan, S. P.; Jiang, Z. H. *Inorg. Chem.* **2005**, *44*, 911. (b) Lu, Y. L.; Wu, J. Y.; Chan, M. C.; Huang, S. M.; Lin, C. S.; Chiu, T. W.; Liu, Y. H.; Wen, Y. S.; Ueng, C. H.; Chin, T. M.; Hung, C. H.; Lu, K. L. *Inorg. Chem.* **2006**, *45*, 2430.

(9) (a) Luo, F.; Long, G. J.; Che, Y.-X.; Zheng, J.-M. *Cryst. Growth Des.* **2008**, *8* (10), 3511. (b) Feng, X.; Zhao, J. S.; Wang, L.-Y.; Shi, X.-G. *Inorg. Chem. Commun.* **2009**, *12*, 388. (c) Zhai, B.; Yi, L.; Wang, H.-S.; Zhao, B.; Cheng, P.; Liao, D. Z.; Yan, S. P. *Inorg. Chem.* **2006**, *45*, 8471.

(10) Zhou, X. P.; Ni, W. X.; Zhan, S. Z.; Li, D.; Yin, Y. G. *Inorg. Chem.* **2007**, *46*, 2345.

(11) (a) Li, B.; Gu, W.; Zhang, L. Z.; Qu, J.; Ma, Z. P.; Liu, X.; Liao, D. Z. *Inorg. Chem.* **2006**, *45*, 10425. (b) Hu, X. X.; Pan, C. L.; Xu, J. Q.; Cui, X. B.; Yang, G. D.; Wang, T. G. *Eur. J. Inorg. Chem.* **2004**, *43*, 1566. (c) Orioli, P.; Bruni, B.; DiVaira, M.; Messori, L.; Piccioli, F. *Inorg. Chem.* **2002**, *41*, 4312.

(12) Fang, Q. R.; Zhu, G. S.; Xue, M.; Sun, J. Y.; Sun, F. X.; Qiu, S. L. *Inorg. Chem.* **2006**, *45*, 3582.

(13) (a) Bunzli, J. C. G.; Chopin, G. R. *Lanthanide Probes in Life, Chemical and Earth Sciences*; Elsevier: Amsterdam, 1989; (b) Costes, J.-P.; Nicodème, F. *Chem.—Eur. J.* **2002**, *8*, 3442. (c) Benelli, C.; Gatteschi, D. *Chem. Rev.* **2002**, *102*, 2369.

(14) (a) Sheldrick, G. M. *SHELXS 97, Program for the Solution of Crystal Structure*; University of Göttingen, Germany, 1997; (b) Sheldrick, G. M. *SHELXL 97, Program for the Crystal Structure Refinement*; University of Göttingen, Germany, 1997;(c) Sheldrick, G. M. *SADABS Siemens Area correction Absorption Program*; University of Göttingen: Göttingen, Germany, 1994.

(15) (a) Liu, M. S.; Yu, Q. Y.; Cai, Q. Y.; Su, C. Y.; Lin, X. M.; Zhou, X. X.; Cai, J. W. *Cryst. Growth Des.* **2008**, *8*, 4083. (b) Li, Y.; Zheng, F.-K.; Liu, X.; Zou, W.-Q.; Guo, G.-C.; Lu, C.-Z.; Huang, J.-S. *Inorg. Chem.* **2006**, *45*, 6308.

(16) (a) Zhu, Y. Y.; Sun, Z. G.; Chen, H.; Zhang, J.; Zhao, Y.; Zhang, N.; Liu, L.; Lu, X.; Wang, W.-N.; Tong, F.; Zhang, L. C. *Cryst. Growth Des.* **2009**, *9*, 3228. (b) Mandal, S.; Pati, S. K.; Green, M. A.; Natarajan, S. *Chem. Mater.* **2005**, *17*, 2912.

(17) Cheng, A. L.; Liu, Na.; Yue, Y. F.; Jiang, Y. W.; Gao, E.-Q.; Yan, C.-H.; He, M.-Y. *Chem. Commun.* **2007**, 407.

(18) Li, W.; Wang, X. L.; Song, X.-Y.; Li, L.-C.; Liao, D.-Z.; Jiang, Z. H. *J. Mol. Struct.* **2008**, *885*, 1.

(19) (a) Huang, Y. G.; Wu, M. Y.; Lian, F. Y.; Jiang, F. L.; Hong, M. C. *Inorg. Chem. Commun.* **2008**, *10*, 840. (b) Zheng, S. L.; Tong, M.-L.; Chen, X. M. *Coord. Chem. Rev.* **2003**, *246*, 185. (c) Batten, S. R.; Murray, K. S. *Coord. Chem. Rev.* **2003**, *246*, 103. (d) Batten, S. R.; Neville, S. M.; Turner D. R., *Coordination Polymers: Design, Analysis and Application*; Royal Society of Chemistry: Cambridge, 2008.

(20) Spek, A. L. *PLATON, A Multipurpose Crystallographic Tool*; Utrecht University: The Netherlands, 2006.

(21) (a) Ryzhkin, I. A; Petrenko, V. F. *Phys. Rev. B.* **2000**, *62*, 280. (b) Jeffrey, G. A. *An Introduction to Hydrogen Bonding*; Oxford University Press: Oxford, U. K., 1997; pp 160−180.

(22) (a) Ghosh, S. K.; Bharadwaj, P. K. *Inorg. Chem.* **2003**, *42*, 8250. (b) Ghosh, S. K.; Bharadwaj, P. K. *Inorg. Chem.* **2004**, *43*, 6887.

(23) (a) Xia, J.; Zhao, B.; Wang, H. S.; Shi, W.; Ma, Y.; Song, H. B.; Cheng, P. *Inorg. Chem.* **2007**, *46*, 3450. (b) Fratini, A.; Richards, G.; Larder, E.; Swavey, S. *Inorg. Chem.* **2008**, *47*, 1030.

(24) Feng, X.; Wang, L.-Y; Zhao, J.-S.; Wang, J. G.; Ng, S. W.; Liu, B. Shi, X.-G. *CrystEngComm*, **2010**, DOI: 10.1039/B913977J.

(25) (a) Fratini, A.; Richards, G.; Larder, E.; Swavey, S. *Inorg. Chem.* **2008**, *47*, 1030. (b) Fratini, A.; Swavey, S. *Inorg. Chem. Commun.* **2007**, *10*, 636.

(26) (a) Sykora, R. E.; Khalifah, P.; Assefa, Z.; Albrecht-Schmitt, T. E; Haire, R. G. *J. Solid State Chem.* **2008**, *181*, 1867. (b) Bray, T. H.; Sullens, T. A.; Shvareva, T. Y.; Sykora, R. E.; Haire, R. G.; Albrecht-Schmitt, T. E. *J. Solid State Chem.* **2007**, *180*, 70.

(27) (a) Aizawa, H.; Katsmuta, T.; Komuro, S. *Sensor Actuators, A* **2006**, *126*, 78. (b) Brayshaw, P. A.; Bunzli, J. C. G.; Froidevaux, P.; Harrowfield, J. M.; Kim, Y.; Sobolev, A. N. *Inorg. Chem.* **1995**, *34*, 2068.

(28) Li, Z. F.; Yu, J; Zhou, L; Zhang, H. J.; Deng, R. P. *Inorg. Chem.* **2008**, *11*, 1284.

(29) (a) Yuan, Y.-F.; Cardinaels, T; Lunstroot, K.; Hecke, K. V.; Meervelt, L. V.; Go1rller -Walrand, C.; Binnemans, K.; Nockemann, P. *Inorg. Chem.* **2007**, *46*, 5302. (b) Weng, D. F.; Zheng, X. J.; Chen, X. B.; Li, L. C.; Jin, L. P. *Eur. J. Inorg. Chem.* **2007**, 3410.

(30) (a) Bünzli, J. C. G. *In Lanthanide Probes in Life, Chemical, and Earth, Sciences. Theory and Practice*; Bünzli, J.-C. G., Choppin G. R., Eds.; Elsevier Scientific Publishers: Amsterdam, 1989; Chapter 7; (b) Choppin, G. R.; Peterman, D. R. *Coord. Chem. Rev.* **1998**, *174*, 283.

(31) Sun, Y.-G.; Yan, X.-M.; Ding, F.; Gao, E.-J.; Zhang, W. Z.; Verpoort, F. *Inorg. Chem. Commun.* **2008**, *11*, 1117.

(32) Prodi, L.; Maestri, M.; Ziessel, R.; Balzani, V. *Inorg. Chem.* **1991**, *30*, 3798.

(33) Wang, P.; Ma, J.-P.; Dong, Y.-B.; Huang, R. Q. *J. Am. Chem. Soc.* **2007**, *129*, 10620.

(34) (a) Sun, Y.-Q.; Zhang, J.; Chen, Y.-M.; Yang, G.-Y. *Angew. Chem., Int. Ed.* **2005**, *44*, 5814. (b) Lu, W. G; Su, C. Y.; Lu, T. B; Jiang, L.; Chen, J. M. *J. Am. Chem. Soc.* **2006**, *128*, 34. (c) Wang, C. F.; Gao, E. Q; He, Z.; Yan, C.-H. *Chem. Commun.* **2004**, 720.

(35) de Lill, D. T.; de Bettencourt-Dias, A.; Cahill, C. L. *Inorg. Chem.* **2007**, *46*, 3960.

(36) (a) Gándara, F.; de Andrés, A.; Gómez-Lor, B.; Gutiérrez-Puebla, E.; Iglesias, M.; Monge, M. A.; Proserpio, D. M.; Snejko, N. *Cryst. Growth Des.* **2008**, *8*, 378. (b) Patra, A.; Friend, C. S.; Kapoor, R.; Prasad, P. N. *J. Phys. Chem. B.* **2002**, *106*, 1909. (c) Zhang, J.; Li, Z.-J.; Kang, Y.; Cheng, J.-K.; Yao, Y.-G. *Inorg. Chem.* **2004**, *43*, 8085. (d) Pan, L.; Liu, H.-M.; Lei, X.-G.; Huang, X.-Y.; Olson, D. H.; Turro, N. J.; Li, J. *Angew. Chem., Int. Ed.* **2003**, *42*, 542.

(37) (a) Moore, E. G.; Szigethy, G.; Xu, J.; Pálsson, L. O.; Beeby, A.; Raymond, K. N. *Angew. Chem., Int. Ed.* **2008**, *47*, 9500. (b) Sun, L. N.; Yu, J. B.; Zheng, G. L.; Zhang, H. J.; Meng, Q. G.; Peng, C. Y.; Fu, L. S.; Liu, F. Y.; Yu, Y. N. *Eur. J. Inorg. Chem.* **2006**, *19*, 3962.

(38) Sabbatini, N.; Guardigli, M.; Manet, I.; Bolletta, F.; Ziessel, R. *Inorg. Chem.* **1994**, *33*, 955.

(39) Wijk, M.; Norrestam, R.; Nygren, M.; Westin, G. *Inorg. Chem.* **1996**, *35*, 1077.

(40) (a) Szytula, A.; Hofmann, M.; Leciejewicz, J.; Penc, B.; Zygmunt, A. *J. Alloys Compd.* **2001**, *316*, 58. (b) Ishikawa, N.; Iino, T.; Kaizu, Y. *J. Am. Chem. Soc.* **2002**, *124*, 11440.

(41) (a) Ishikawa, N.; Sugita, M.; Okubo, T.; Tanaka, N.; Iino, T.; Kaizu, Y. *Inorg. Chem.* **2003**, *42*, 2440. (b) Baggio, R.; Garland, M. T.; Peñao.; Perec, M. *Inorg. Chim. Acta* **2005**, *358*, 2332.

(42) (a) Andruh, M.; Bakalbassis, E.; Kahn, O.; Christian Trombe, J.; Porchers, P. *Inorg. Chem.* **1993**, *32*, 1616. (b) Ishikawa, N.; Iino, T.; Kaizu, Y. *J. Phys. Chem. A.* **2002**, *106*, 9543.

(43) Zhang, Z.-H.; Song, Y.; Okamura, T.; Hasegawa, Y.; Sun, W. Y.; Ueyama, N. *Inorg. Chem.* **2006**, *45*, 2896.

(44) (a) Arumuganathan, T.; Das, S. K. *Inorg. Chem.* **2009**, *48*, 496. (b) Zhang, Z.-H.; Okamura, T.; Hasegawa, Y.; Kawaguchi, H.; Kong, L.-Y.; Sun, W. Y.; Ueyama, N. *Inorg. Chem.* **2005**, *44*, 6219. (c) Lam, A. W. H.; Wong, W.-T.; Wen, G. H.; Zhang, X. X.; Gao, S. *New J. Chem.* **2001**, *25*, 531.

(45) Kahn. O. *Molecular Magnetism*; VCH Publishers: New York, 1993.

(46) (a) Stamatatos, T. C.; Foguet-Albiol, D.; Lee, S. C. *J. Am. Chem. Soc.* **2007**, *129*, 9484. (b) Plass, W.; Fries, G. *Z. Anorg. Allg. Chem.* **1997**, *623*, 1205. (c) Panagiotopoulos, A.; Zafiropoulos, T. F.; Perlepes, S. P.; Bakalbassis, E.; Masson-Ramade, I.; Kahn, O.; Terzis, A.; Raptopoulou, C. P. *Inorg. Chem.* **1995**, *34*, 4918. (d) Liao, Y.; Shum, W. W.; Miller, J. S. *J. Am. Chem. Soc.* **2002**, *124*, 9336.

(47) Blanusa, J.; Mitric, M.; Felner, I.; Jovic, N.; Bradaric, I. *J. Magn. Magn. Mater.* **2003**, *263*, 295.

(48) (a) Costes, J. P.; Nicodème, F. *Chem.—Eur. J.* **2002**, *8*, 3442. (b) Zhao, H.; Bazile, M. J.; Galán-Mascarós, J. R.; Dunbar, K. R. *Angew. Chem., Int. Ed.* **2003**, *42*, 1015. (c) Hatscher, S. T.; Urland, W. *Angew. Chem., Int. Ed.* **2003**, *42*, 2862. (d) Ishikawa, N.; Otsuka, S.; Kaizu, Y. *Angew. Chem., Int. Ed.* **2005**, *44*, 731.